THE ASTROPHYSICAL JOURNAL, 430:495–504, 1994 August 1

THE INTERMEDIATE LINE REGION OF QSOs

M. S. BROTHERTON AND BEVERLEY J. WILLS
McDonald Observatory and Astronomy Department, University of Texas, Austin, TX 78712;
msb@astro.as.utexas.edu, bev@astro.as.utexas.edu

PAUL J. FRANCIS[1]
Steward Observatory, University of Arizona, Tucson, AZ 85721

AND

CHARLES C. STEIDEL[2,3]
Astronomy Department, University of California, Berkeley, CA 94720
Received 1993 October 28; accepted 1994 January 27

ABSTRACT

Our recent statistical investigations of broad UV lines of luminous QSOs suggest that the traditional broad-line region (BLR) consists of two components—one of width ~ 2000 km s^{-1} FWHM with the peak within a few hundred kilometers per second of the systemic redshift, and another very broad component of width ≥ 7000 km s^{-1} FWHM and blueshifted by ≥ 1000 km s^{-1}. Differences in the relative strengths of these components account for much of the diversity of broad-line profiles, as well as relations among line strength, line width, asymmetry, and peak blueshift. We have suggested that the narrower component arises in a distinct intermediate-line region (ILR) that is an inner extension of the narrow-line region (NLR).

We form spectra of the ILR and very broad line region (VBLR) in two complementary ways. First, using a small sample of high-quality spectra, we difference two composite spectra, one with FWHM$_{\rm C\,IV} \sim 3000$ km s^{-1}, the other with FWHM$_{\rm C\,IV} \sim 7000$ km s^{-1} (essentially a VBLR spectrum)—revealing a narrower line spectrum with FWHM ~ 2000 km s^{-1}. Second, we use a principal component analysis of 200 low signal-to-noise ratio spectra from the Large Bright Quasar Survey. The ILR is identified with the first principal component—that component accounting for most of the spectrum-to-spectrum variation. The VBLR spectrum is derived by subtracting this ILR from the mean spectrum. The two methods yield similar results, and the spectra of the ILR and VBLR are very different. Additional support for the existence of two components is the lack of a correlation between the equivalent widths of the ILR and VBLR.

We discuss the relationships between the VBLR, the ILR, and the traditional NLR. The ILR line intensity ratios are distinctly different from those of the VBLR, with (relative to C IV λ1549) stronger Lyα and weaker N V λ1240, λ1400 feature, He II λ1640, O III] λ1663, and Al III λ1860. Comparison with other AGN emission-line regions shows that the ILR spectrum tends to be intermediate between that of the VBLR and that of gas more distant from the ionizing continuum, such as the NLR and extended Lyα nebulosity. Comparison of the spectra with results from photoionization models suggests that, compared with the VBLR, the ILR is about 10 times more distant from the ionizing continuum (~ 1 pc), 100–1000 times less dense (10^{10} cm^{-3}), and has a smaller covering factor ($\lesssim 3\%$, compared with $\sim 24\%$ for the VBLR).

Subject headings: line: profiles — quasars: emission lines — quasars: general

1. INTRODUCTION

Even from the time of the earliest attempts to explain AGNs' broad emission line spectra by photoionization, it was recognized that simple single-zone models were inadequate (Ferland 1987; Netzer 1985). Now the evidence is very clear: for example, different redshifts and different response times to continuum variations for high- and low-ionization lines, and anomalous line strengths. We have accepted the quixotic challenge of Ferland (1986) to separate the broad-line region (BLR) into distinct regions.

New statistical investigations of QSO broad UV lines (Francis et al. 1992; Wills et al. 1993; Brotherton et al. 1994—see also Baldwin et al. 1988) have led us to propose that the next order of sophistication is a two-component model: a high-density very broad line region (VBLR) and a lower density intermediate-line region (ILR) of velocity dispersion intermediate between those of the traditional narrow-line region (NLR) and the VBLR. The BLR comprises the ILR and VBLR. To a good approximation, the ILR gives rise to a line component of 2000 km s^{-1} FWHM at the systemic redshift, while the VBLR gives rise to a component of 7000 km s^{-1} FWHM with a blueshift of 1000 km s^{-1}. We have argued that the ILR may simply be an inner extension of the NLR.

A crucial element of this two-component model is that the relative contributions of the ILR and VBLR vary from one QSO to another, with a larger disperson in the equivalent width of the ILR component. Because the ILR and VBLR give rise to spectra having different line ratios, the ratio of ILR to VBLR contribution is different for different lines and determines their different line shapes. If we use the observed and modeled NLR line ratios (Ferland 1986) relative to those of typical BLR spectra as a rough guide to the line strengths of the ILR relative to those of the VBLR, we expect that Lyα will be dominated by ILR emission, and that C IV λ1549 will have a

[1] Current address: School of Physics, University of Melbourne, Parkville, Victoria 3052, Australia; pjf@tauon.ph.unimelb.edu.au.
[2] Hubble Fellow.
[3] Current address: Physics Department, Massachusetts Institute of Technology, Room 6-201, Cambridge, MA 02139; steidel@alioth.mit.edu.

very significant ILR contribution; Hβ should be dominated by VBLR emission, and so should the higher ionization lines of N v λ1240 and Si iv λ1397. This leads naturally to the following correlations with FWHM:

1. The strong anticorrelation between equivalent width (EW) and FWHM for C iv λ1549;
2. The anticorrelation between EW and FWHM for Lyα;
3. The positive correlation between EW and FWHM for the λ1400 feature—and also for Hβ;
4. The negative correlation between the line intensity ratio Lyα/C iv and FWHM;
5. The positive correlation of the line intensity ratio N v λ1240/C iv with FWHM (not independent of item 1);
6. The positive correlation of the line intensity ratio λ1400/C iv with FWHM (not independent of items 1 and 3);
7. The more peaked profiles of narrower C iv lines relative to broader C iv lines;

The relative blueshift of the VBLR line component leads naturally to:

8. The increasing blueshift of C iii] λ1909, C iv, and λ1400 feature with increasing FWHM;
9. The form of the dependence of C iv line asymmetry with FWHM.

All these relations and some others are observed in the expected sense. Item 1, together with item 9, was the observational relation that originally led to the idea of the ILR-VBLR model (Wills et al. 1993). Correlations 3, 6, and 7 are presented by Wills et al. (1993). Brotherton et al. (1994) present and discuss correlations for the C iii] λ1909 line, including item 8. Most of these, and other correlations, are implicit in the principal component analysis presented by Francis et al. (1992).

The two-component model provides the simplest self-consistent interpretation of these observations. We are not sure to what extent the ILR and VBLR are truly distinct regions (see § 4.3). However, there are clearly independently varying contributions from regions with the properties we attribute to ILR and VBLR gas, and this fact forms the basis of our simple model. Another possible interpretation of some of these relations in terms of orientation was attempted by Wills et al. (1993), but required the introduction of further ad hoc parameters, and so was rejected, for the time being, in favor of the simpler ILR-VBLR model. In any case, if we are able to show that the characteristic spectra are different for low- and high-velocity gas, models dependent only on orientation of an axisymmetric velocity field are ruled out.

We emphasize that we present a straw-man model as a step toward more realistic representations of the BLR. Note that the simplest two-component model, in which the ILR and VBLR are homogeneous regions, is already ruled out because, for C iii] from the VBLR alone, there appears to be a relation between blueshift and line width (Brotherton et al. 1994).

It is the purpose of the present paper (1) to show that broad- and narrow-line objects have systematically different line ratios, (2) to derive the different emission-line properties of the ILR and VBLR, and (3) to compare the ILR and VBLR spectra with each other, with other types of AGN spectra, and with results of photoionization models, as steps toward understanding the physical conditions and origins of these regions.

We pursue this investigation using complementary methods with two high-redshift data sets. The first, the absorption-line sample (hereafter ALS), is selected from a heterogeneous sample of luminous QSOs with spectra of high signal-to-noise ratio originally obtained to study absorption-line systems (Sargent, Boksenberg, & Steidel 1988; Sargent, Steidel, & Boksenberg 1989; Steidel & Sargent 1991, 1992; Sargent & Steidel 1994; Wills et al. 1993; Brotherton et al. 1994). The second data set (hereafter LBQS) is derived from the Large Bright QSO Survey, a homogeneous optically selected sample of over 1000 QSOs which is believed to be nearly complete, but with lower signal-to-noise ratio spectra than the ALS (Foltz et al. 1987, 1989; Hewett et al. 1991; Chaffee et al. 1991; Morris et al. 1991; Francis et al. 1992).

2. THE DERIVATION OF ILR AND VBLR SPECTRA

2.1. *The ALS*

Using the spectra of a sample of ~190 predominantly radio-quiet AGNs with $1.1 \leq z \leq 3.3$ from the ALS, we have constructed spectra distinguished by the width of the C iv λ1549 emission line. One is a narrow-lined composite, formed using 16 objects with 2500 km s^{-1} ≤ FWHM$_{\rm C\,IV}$ ≤ 3500 km s^{-1}. The other is a broad-lined composite formed using 15 objects with 6000 km s^{-1} ≤ FWHM$_{\rm C\,IV}$ ≤ 8000 km s^{-1}. Both subsamples cover a similar range in optical luminosity and redshift. Our previous work has shown that the narrow-lined composite is dominated by the ILR and that the broad-lined composite is essentially pure VBLR.

The individual spectra we use do not cover the entire wavelength region of interest (from Lyα to C iii] λ1909), although C iv λ1549 appears in all spectra. Before combining, each spectrum has been corrected for Galactic reddening and then normalized by dividing by the continuum. The average continuum for both subsamples is well approximated by $f_\nu \propto \nu^{-0.5}$. For these data, the resolution (~400 km s^{-1}) and signal-to-noise ratio (≳20 in the continuum) are sufficient to allow us to remove narrow absorption lines prior to combination. The smallest reasonable correction for Lyα absorption has been made, consistent with line profiles being smooth. Thus the true absorption in Lyα has been underestimated. Rest wavelength scales have been determined from the peak of the C iv line. Our previous work has shown that the VBLR is blueshifted by ~1000 km s^{-1} relative to the ILR, so we have shifted the broad-lined composite by this amount. We note that this places the peaks of the low-ionization lines of O i λ1304 and C ii λ1335 at the same wavelengths in both the broad- and narrow-lined composites.

We have subtracted the broad-lined composite from the narrow-lined composite to produce a difference spectrum. Because the equivalent widths of the VBLR do not appear to depend on linewidth, i.e., the ILR and VBLR component strengths appear to be independent, the VBLR contribution tends to cancel, resulting in an emission-line spectrum representative of the ILR alone.

In Figures 1*a* and 1*b* we overplot our continuum-normalized broad- and narrow-lined composites, with the standard deviation spectra shown immediately beneath. The difference spectrum is shown in the lower panel. In Table 1 we present measurements of the emission lines: the EWs, FWHMs, and the line peaks. For all lines, a local continuum was assigned interactively and the flux density integrated to give the EWs. No deblending was attempted for the measurements in Table 1. The line-peak wavelengths refer to the flux-weighted mean above a level 85% of the line peak, and these measurements of the broad-lined composite were made *after* blueshifting it 1000 km s^{-1}.

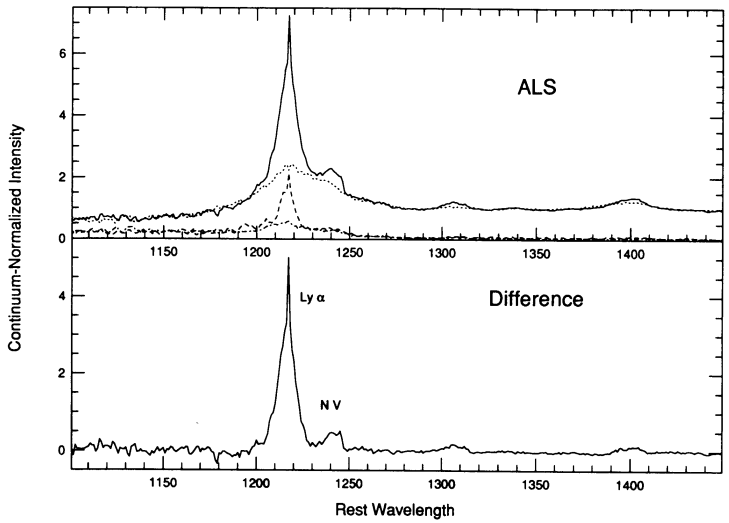

FIG. 1*a*

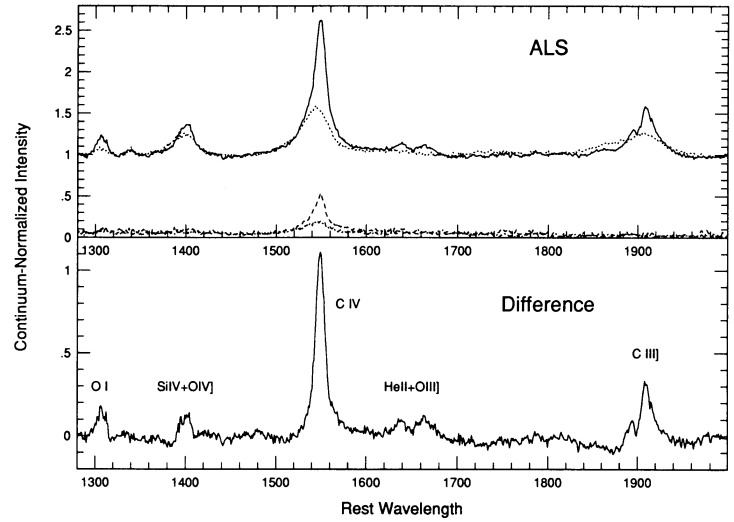

FIG. 1*b*

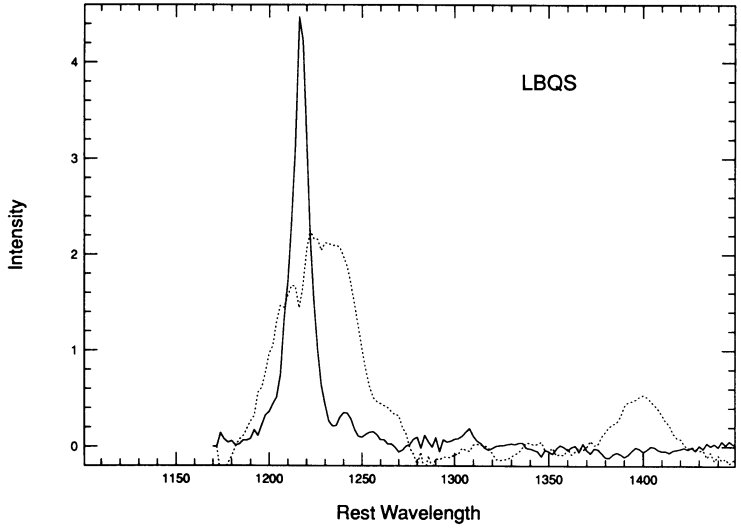

FIG. 1*c*

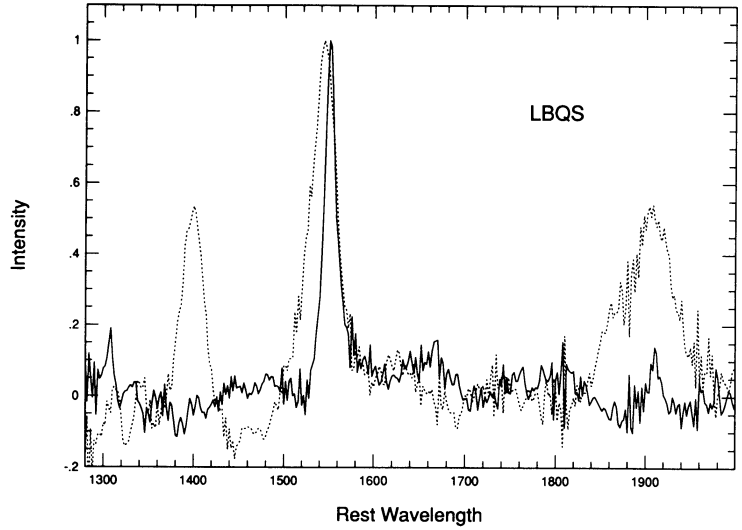

FIG. 1*d*

FIG. 1.—(*a*) Narrow-lined (*solid*) and broad-lined (*dotted*) continuum-normalized "EW spectra" of the Lyα region from the ALS are shown with their standard deviation spectra. Below, the difference spectrum is displayed. (*b*) Same as (*a*), for the C IV region. (*c*) Continuum-subtracted F_λ ILR (*solid*) and VBLR (*dotted*) spectra of the Lyα region from the LBQS. The spectra are normalized such that C IV peaks at unity. (*d*) Same as (*c*), for the C IV region.

TABLE 1

EMISSION LINE PROPERTIES OF ALS COMPOSITES[a]

Property	Ly α + N V[b]	O I	C II	Si IV + O IV]	C IV	He II + O III]	C III][c] + Al III
EW:							
Narrow	100±10	2.9±0.2	0.7±0.1	9.6±1.0	41±4	9±1	20±2
Broad(VBLR)	55±4	1.0±0.1	0.9±0.1	8±1	21±1	6±1	17±2
Difference(ILR)[d]	39.4±1,3.9±0.2	2.0±0.1	<0.1	1.8±0.2	18.3±0.7	1.7±0.2, 2.4±0.6	6.2±0.5
FWHM:							
Narrow	2700±200	2900±200	2500±200	4500±200	3100±100	···	3200±200
Broad(VBLR)	11000±600	3800±500	2800±300	5800±500	6800±300	···	8900±1000
Difference(ILR)	1400±100, 2400±200	2500±400	···	4400±200	2400±200	···	1700±100
Peak Wavelength:							
Narrow[e]	1217.2±0.2, 1241.8±0.2	1306.5±0.1	1338.5±1.0	1401.8±0.2	1549.1±0.1	1640.1±0.3, 1663.3±0.2	1908.7±0.2, 1860.5±1.0
Broad(VBLR)[f]	1217, 1238.5	1305.5±0.3	1339.8±0.5	1399.2±0.4	1544.1±0.1	···	1904.0±0.8, ···
Difference(ILR)	1217.2±0.2, 1242.4±0.4	1306.3±0.3	···	1394.5±0.4, 1403.0±0.2[g]	1549.2±0.1	1639.5±0.5, 1663.3±0.3	1908.8±0.1, ···

[a] The errors are the estimated errors in continuum placement and do not represent those associated with the construction of the composite spectra. Our estimated line ratios of blends are given in Table 2. EWs and line-peak positions are in angstroms, FWHMs are in km s^{-1}.

[b] Using a Gaussian deblending procedure for the VBLR spectrum, FWHM Lyα = 8000 ± 600 km s^{-1} after removing N v. The line positions given correspond to the peaks of the Gaussian components.

[c] Si III] λ1892 is apparently resolved in the narrow-lined composite and difference spectrum, but its flux is included with C III] λ1909.

[d] When two values are given, they represent measurements of the individual species constituting the blend.

[e] Rest wavelength scale is defined by the peak of C IV λ1549.

[f] Rest wavelength scale is defined by the peak of C IV λ1549; the spectrum has then been blueshifted by 1000 km s^{-1}, and the listed line positions include this shift.

[g] The peaks of the λ1400 feature are derived from a two-Gaussian fitting routine.

2.2. *The LBQS*

We used a subsample of 200 LBQS QSOs having spectra covering the entire rest-frame wavelength range 1175–2000 Å and having no obvious broad absorption lines (BALs) or strong associated absorption. Given the relatively low signal-to-noise ratio of the LBQS spectra, it is likely that some QSOs with absorption lines were still included. The rest wavelength scale of each spectrum was determined by cross-correlation with a high signal-to-noise ratio composite. No radio measurements are available for most of the sample, but only 10% are expected to be radio-loud (Hooper, Impey, & Hewett 1994; Visnovsky et al. 1992). All spectra are normalized to unit flux density at 1450 Å, and a linear continuum was subtracted from each.

We used the linear correlation technique of principal component analysis (PCA; see Francis et al. 1992; Mittaz, Penston, & Snijders 1990) to separate the narrow and very broad component spectra. There are qualitative differences between this analysis and that of Francis et al. (1992): the subtraction of the continua and exclusion of BALQSOs essentially eliminates the second and third principal components present in the results of Francis et al. (1992), although our remaining components are similar to the higher order components reported there.

Essentially, the first principal component, which accounts for about $\frac{2}{3}$ of the spectrum-to-spectrum variation, may be identified with the spectrum of the ILR. To get a spectrum of the VBLR, we subtracted as much of this "first principal component spectrum" as possible from the mean spectrum while leaving it smooth (i.e., without dips due to the subtraction of the narrower component). This spectrum does indeed closely resemble the broadest lined individual spectra, giving us confidence that our technique is appropriate.

The first principal component spectrum does not necessarily represent a pure ILR spectrum for two reasons. First, because the PCA technique separates orthogonal (independent) components, if the ILR and VBLR components are correlated, the first principal component spectrum could include a contribution from the very broad component. The second reason is more technical: PCA will identify components that are orthogonal functions of the *observed* quantities, namely the flux densities at the line centers and at larger radial velocities (the wings of the emission lines). So, even if the ILR and VBLR are totally uncorrelated, the observed quantities will not be, as both the ILR and the VBLR contribute to the flux densities in the line centers. Thus, the first principal component spectrum may contain a small contribution from the VBLR. For these reasons, we subtract as much of our VBLR spectrum as possible from the first principal component spectrum, in an attempt to produce a pure ILR spectrum. In practice, very little VBLR spectrum can be subtracted before the line wings show "absorption." The LBQS ILR and VBLR spectra are shown in Figures 1*c* and 1*d*.

The success of the ILR and VBLR spectra in describing the diversity of real QSO spectra is discussed by Francis, Brotherton, & Wills (1994). They derive EWs of VBLR and ILR contributions by fitting templates to individual LBQS QSOs and find no correlation between them, confirming that the PCA technique identifies two independently varying components.

Mittaz et al. (1990) use PCA on samples of simulated spectra in which the strengths and widths of single-component emission lines are varied. We have conducted our own simulations with artificial spectra, each composed of single Gaussian representations of Lyα and C IV that behave like our data with respect to the observed relations among EW, line ratios, and FWHM. We find no significant difference between the first principal component spectrum of the simulation and that of the LBQS. Given the size and signal-to-noise ratios of this data set, we conclude that, based on the first principal component, PCA cannot *easily* disprove a single-zone model designed to reproduce all the observed correlations. However, PCA does serve as a valid and complementary approach to understanding the correlations and to the derivation of the ILR and VBLR spectra.

2.3. *Comparison of ALS and LBQS Spectra*

In Figures 2*a* and 2*b* we plot the ALS and LBQS ILR and VBLR spectra on F_λ scales (correcting the continuum-normalized spectra of Fig. 1 using the average continuum). These spectra are normalized by scaling the peak of C IV to unity, to allow direct comparison of the two samples. There is good general agreement. Some differences are probably a result of the differences in data quality. For instance, the stronger Lyα in the ALS may be partially attributed to the removal of absorption lines in those spectra. Also, differences in the definition of the rest wavelength scale of the VBLR spectra of the ALS and LBQS may result in different apparent Lyα/N V λ1240 ratios in our deblending. Real differences may arise because the ALS QSOs are on average 6 times more luminous than the LBQS QSOs. We note that only two objects are in common between the 31 ALS QSOs and the 200 LBQS QSOs used to construct our composite spectra (QSOs 0101−304 and 1244+1129, both with 6000 km $s^{-1} \leq$ $\mathrm{FWHM}_{\mathrm{C\,IV}} \leq 8000$ km s^{-1}).

In Table 2, we give the line intensity ratios of our composite spectra, the derived ILR and VBLR spectra from both the ALS and LBQS, and, for comparison, line ratios from other sources. We have used Gaussian fitting to measure the relative contributions of blended lines. Single Gaussians worked well for N V, C III], and Al III, but two Gaussians each were required for Lyα and C IV, a narrow one at the line peak and a broader blue-shifted one, for both the ILR and VBLR spectra. Continuum windows and initial guesses for Gaussian parameters were chosen consistently for measurements of both the ILR and VBLR spectra of both the ALS and LBQS samples.

3. RESULTS

3.1. *Comparison of the ILR and VBLR Spectra*

In addition to the line-width differences between the ILR and VBLR spectra, there exist some unambiguous differences between the line ratios of the ILR and VBLR (Table 2): relative to C IV, the ILR has weak N V λ1240, λ1400 feature, and Al III λ1860. Other smaller differences are that, relative to C IV, the ILR has strong Lyα and weak C III] λ1909. The line ratio differences are clearly seen in Figure 3, where we compare the entire ILR and VBLR spectra from the ALS, plotted such that the peak of C IV is normalized to unity.

In the case of the ALS ILR spectrum, the lines are fairly symmetric and the redshift scale is well defined. This redshift is believed to be systemic (Brotherton et al. 1994; and § 4.3).

Francis et al. (1994) find that the linear EW distributions of the LBQS VBLR and ILR emission lines are rather different. The VBLR EWs are normally distributed, while the ILR distribution is well described by an exponential function of the form $n(\mathrm{EW}) \propto e^{-\mathrm{EW}/\langle \mathrm{EW} \rangle}$. However, if the ILR and VBLR distributions are plotted in log EW, their shapes are approx-

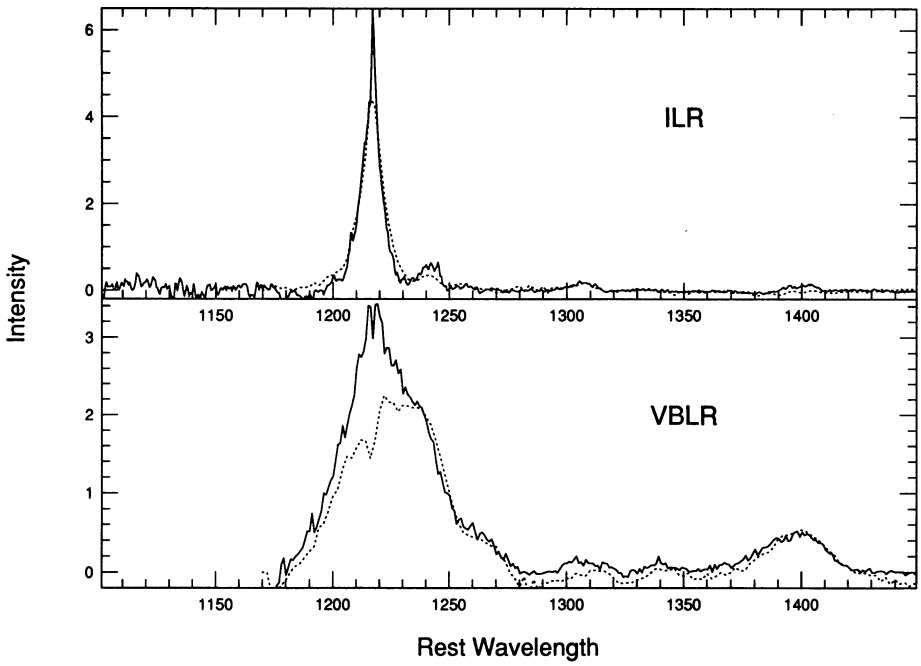

FIG. 2a

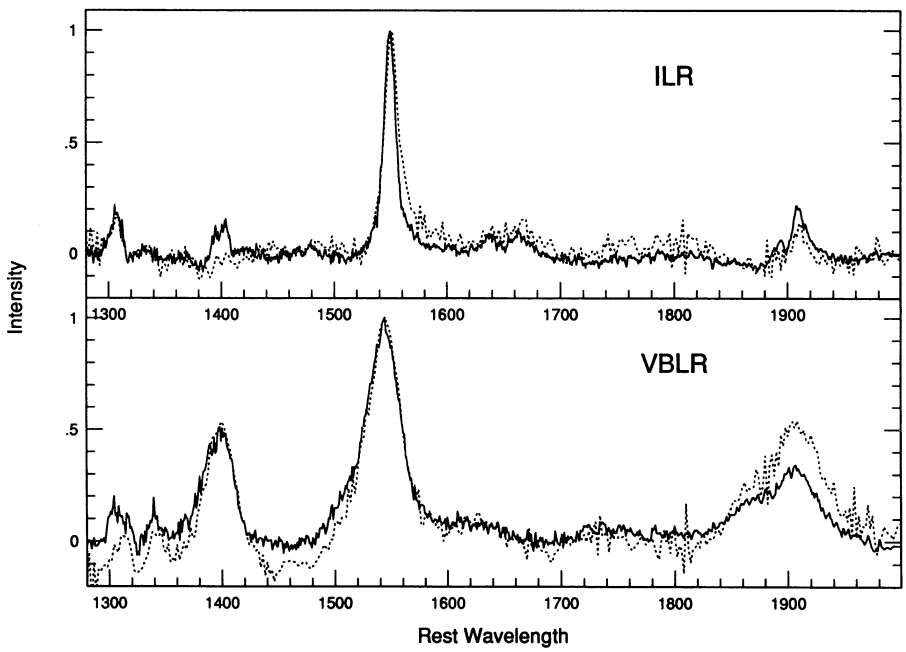

FIG. 2b

FIG. 2.—(*a*) ALS (*solid*) and LBQS (*dotted*) spectra of the ILR and VBLR are compared for the Lyα spectral region. The ILR spectra are shown above the VBLR spectra. For the comparison of line ratios, all spectra are on the same intensity scale (continuum-subtracted F_λ, multiplied by a factor to make C IV peak at unity). (*b*) Same as (*a*), but for the C IV spectral region.

imately symmetric and similar for both broad and narrow lines, but the ILR distribution is 3 times broader than that for the VBLR.

3.2. *The λ1400 Feature in the ALS ILR Spectrum*

The ILR λ1400 feature shows two peaks, also seen in some individual spectra, near the expected wavelengths of the O IV] λ1402 and Si IV λ1394 and λ1403 doublet lines (see Table 1). We have attempted to deblend Si IV and O IV]. We model O IV] using the five strongest lines of the multiplet, and Si IV using its two lines. We used statistical weight ratios for the Si IV doublet at low density, and equal weighting for high density; density-dependent O IV] multiplet ratios were taken from Nussbaumer & Storey (1982). We allowed the Si IV to

TABLE 2

LINE INTENSITY RATIOS

Spectrum	Lyα λ1216	NV λ1240	SiII λ1263	OI λ1305	CII λ1335	SiIV+OIV] λ1397+λ1402	CIV λ1549	HeII+OIII] λ1640+λ1663	AlIII λ1859	SiIII] λ1892	CIII] λ1909
ALS VBLR	219	111	31	10	6	42	100	31 + 0	17	<5	41
LBQS VBLR	154	137	16	7	6	55	100	40 + 0	22	...	59
ALS ILR	289	34	7	15	6	12	100	9 + 13	0	5	31
LBQS ILR	254	11	3	15	6	3	100	50	0	...	25
NLQSO[a]	340	20	...	...	...	20	100	10 + <5	...	...	20
Mean Seyfert 2[b]	458	...	...	...	...	...	100	...	...	...	46
NGC 1068[c]	207	61	4.8	2.5	8	23	100	54 + 6	...	...	67
NGC 1068 Dereddened[c]	354	101	7.4	3.5	11	29	100	46 + 6	...	...	46
NL Radio Galaxies[d]	852	42	...	...	10	45	100	87 + 20	...	...	49
QSO Nebulae[e]	1430	<72	...	...	...	<72	100	143:	...	...	72:
McCarthy Model[f]	1312	2	...	...	8	7	100	73 + 8	...	...	68
NLR Model[g]	312	3	...	...	1.3	3 + 4	100	... + 9	...	4.9	57
VBLR Model[h]	238	15	...	2	3	35 + 3	100	37 + 1	13	3	0
ILR Model[h]	254	1	...	2	2	12 + 3	100	7 + 14	3	7	19

[a] Representative narrow-lined QSO spectrum from Baldwin et al. 1988.
[b] From Ferland & Osterbrock 1986, reddening-corrected.
[c] From Kriss et al. 1993.
[d] From the high-z composite by McCarthy 1993.
[e] From Heckman et al. 1991.
[f] Photoionization model from McCarthy 1993, calculated with CLOUDY, $n = 100\ \mathrm{cm}^{-3}$, $\log U = -1.8$.
[g] Representative NLR photoionization model from the appendix by Ferland 1993.
[h] The VBLR and ILR CLOUDY photoionization models using the "agn" continuum, as described in the text.

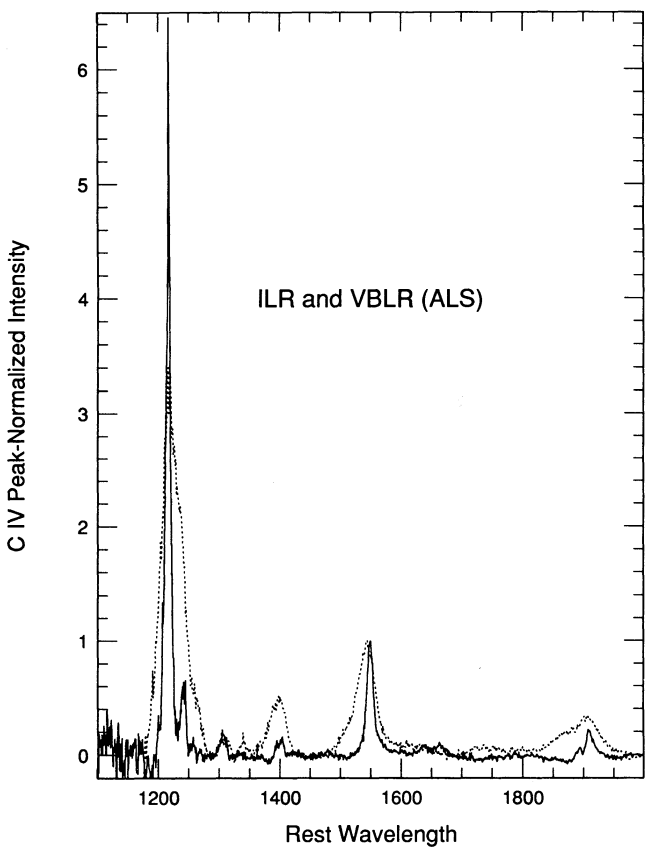

FIG. 3.—ALS ILR (*solid*) and VBLR (*dotted*) spectra from Fig. 2 are compressed to show the entire UV wavelength range.

O IV] intensity ratio to vary and ran models using both the ILR C IV profile and a Gaussian of unconstrained width as a line template for both high-density (10^{11} cm^{-3}) and low-density ($<10^{9}$ cm^{-3}) cases. The C IV profile proved too broad to fit the observed peaks, but, for both the high- and low-density models, a Gaussian of about 1500 km s^{-1} gave good fits. The high-density model indicated Si IV/O IV] ~ 2, while the low-density model gave a ratio of ~1. Based on our analysis of the ILR spectrum (§ 4.2), the lower density value seems more appropriate. See Wills et al. (1993) and references therein for other results.

4. DISCUSSION

4.1. *Comparisons with Other AGN Spectra*

Table 2 compares the relative strengths of UV lines in the ILR and VBLR spectra with those of other AGN emission-lines regions and models. The narrow-lined QSO (NLQSO) spectrum is representative of three objects with especially narrow broad-lines investigated by Baldwin et al. (1988). A reddening-corrected Seyfert 2 composite is from Ferland & Osterbrock (1986). Unfortunately, few UV lines have been detected in Seyfert 2 nuclei, so we include the narrow-line ratios of NGC 1068 (Kriss et al. 1993). A composite spectrum for narrow-line radio galaxies is taken from McCarthy (1993). We also include the spectrum of the extended Lyα nebulosity; this may be like the spectra of extended nebulae around high-redshift radio galaxies (Heckman et al. 1991). For comparison we include line ratios from two CLOUDY NLR models, one from McCarthy (1993) and the other from Ferland (1993).

A complication in making these comparisons is the unknown reddening by dust, especially for UV-only spectra where there are no reliable reddening indicators; at least lines

nearby in wavelength can be compared. Fortunately the line ratios shown for low-redshift Seyfert 2s are corrected for reddening. Their observed variation in reddening from object to object is sufficiently large that a composite would otherwise be meaningless (Ferland & Osterbrock 1986). The narrow-line ratios for NGC 1068 are given with and without correction for reddening. However, reddening corrections are not available for spectra of high-redshift objects.

All ILR line ratios are like those of the NLQSOs despite the not insignificant contribution of the VBLR to the latter. We identify our ILR with the 1500 km s^{-1} "narrow" emission line region of the NLQSOs, as anticipated by Baldwin et al. (1988).

Clearly, the intensity ratio Lyα/C IV for the ILR is larger than for the VBLR. The ratio increases from Seyfert NLRs through high-redshift radio galaxies, to extended Lyα emission nebulosities, and so appears to increase with increasing distance of the gas from the central AGN. The high ratio Lyα/N V $\sim$10–20 for the ILR is much larger than that for the VBLR, and more similar to that for more extended regions. The ratios C III]/C IV and λ1400/C IV for the ILR are low compared with all other AGN emission spectra shown—perhaps an indication of higher densities compared with gas more distant from the nucleus.

4.2. *Comparisons with Models*

We compare our ILR and VBLR emission-line ratios with values from photoionization models. We assume solar metallicity and that the ILR and VBLR see the same ionizing continuum source, with no shadowing. Using CLOUDY (Ferland 1993) we have calculated detailed grids of models covering a range of hydrogen density, n_H, from 10^9 to 10^{14} cm^{-3} and Φ from 10^{17} to 10^{23} s^{-1} cm^{-2}, where Φ is the flux of hydrogen-ionizing photons incident on the gas. It is convenient to use Φ rather than the more conventional ionization parameter $U = \Phi/(n_H c)$, because the distance, r, of the ionized gas from the continuum can be determined directly from $\Phi \propto L/r^2$, given the source luminosity L. We have tried two continua—CLOUDY's "agn" continuum, which is the Mathews & Ferland (1987) continuum modified to have a submillimeter break at 10 μm, and the "agn1" continuum designed to maximize the relative intensity of N V λ1240 (Baldwin et al. 1994). We have compared specific CLOUDY models with the results from the photoionization code ION (e.g., Rees, Netzer, & Ferland 1989) using the Mathews & Ferland (1987) continuum. Both codes gave similar results. The numbers we quote below and in Table 2 are from our CLOUDY model using the "agn" continuum.

For both the ILR and VBLR spectra, N V λ1240/C IV λ1549 is observed to be large compared with the predicted model values using parameters yielding good agreement with other line ratios. Hamman & Ferland (1992) suggest that this is probably an indication of high metallicity in high-redshift, high-luminosity QSOs and show that increasing the metallicity of photoionization models can achieve a high N V λ1240/C IV λ1549 ratio without changing the other line ratios significantly.

For the ILR spectrum, line ratios are in general agreement with models in which $n_H \approx 10^{10}$ cm^{-3} and $\Phi \approx 10^{18.5}$ s^{-1} cm^{-2} ($U = 0.01$, ILR model in Table 2). The best "agn1" model had a higher $\Phi \approx 10^{19.0}$ s^{-1} cm^{-2}.

Most VBLR emission-line ratios are in general agreement with models having $n_H \approx 10^{12.5}$ cm^{-3} and $\Phi \approx 10^{21}$ s^{-1} cm^{-2} ($U = 0.01$, VBLR model in Table 2). There is one major exception: C III] λ1909/C IV λ1549 has an observed value too large for these parameters by at least an order of magnitude. This may indicate that our two-component description of the BLR is too simple and that the VBLR itself is not well described as a single homogeneous region. This was suggested by Brotherton et al. (1994) because of their finding that, for the VBLR, blueshift increases with increasing line width. The strength of C III] is also a severe problem for the dynamical models of a photoionized BLR investigated by Kallman et al. (1993). The significant amount of C III] VBLR emission, probably related to its large line width relative to other lines (Brotherton et al. 1994), may conflict with the results of variability studies where the claimed time lag of the C III] λ1909 intensity following continuum variations suggests that C III] comes from the outer regions of the BLR (e.g., Clavel et al. 1991; Krolik et al. 1991). However, this claimed result is for AGNs of much lower luminosity.

Models with a lower density wind arising from VBLR clouds (similar to those proposed by Baldwin et al. 1994) might be able to account for the high C III]/C IV line ratio we observe. Another possible solution may lie in the fact that C III] is semiforbidden; perhaps the profiles of permitted lines are modified by absorption. More investigation is required.

These model parameters indicate that the VBLR is roughly 100–300 times denser and 10–20 times closer to the central engine than is the ILR, in general agreement with the expectation that both velocity and density decrease with increasing distance from the center of AGNs. In fact, if $n_H \propto r^{-s}$ we derive $s = 2$, consistent with the ionization parameter being independent of r. We also find that velocity (as measured by FWHM), $v \propto r^{-1/2}$, as expected, for example, in the case of bound Keplerian motion. See Rees et al. (1989) for models of the dependence of line strength and profiles on different power laws describing the behavior of velocity and density with radius.

Assuming $H_0 = 50$ km s^{-1} and $q_0 = 0$, our ALS QSOs have a mean $M_B = -28.2$. Using the "agn" model continuum, we calculate the flux of ionizing photons as a function of distance from a central continuum source and compare this with the model values of Φ for the ILR and VBLR, to derive VBLR and ILR distances of 0.07 and 1.2 pc, respectively. The above power-law dependences of density and velocity on distance are roughly consistent with extrapolations to typical distances and densities of the NLR.

Comparing the model EW of C IV with our observed values (from Table 1), we calculate a covering factor, $\Omega/4\pi$, of 0.03 for the ILR and 0.24 for the VBLR. The observed EW is derived for QSOs with a dominant ILR component. In QSOs dominated by the VBLR, significantly weaker ILR spectra would lead to correspondingly smaller covering factors. These covering factors may be compared with typical covering factors for NLR gas of $\lesssim$0.02, based on simple photoionization models and observed line strengths in lower luminosity QSOs. Note that Netzer & Laor (1993) suggest that narrow-line emission may be suppressed by dust, allowing the actual covering factor of the NLR to be higher.

4.3. *The Nature of the ILR and the VBLR*

Because the line cores are narrow ($\sim$2000 km s^{-1}), Wills et al. (1993) suggested that the ILR is a high-velocity, inner extension of the NLR. In support of this are:

1. The ILR emission lines are apparently at the systemic redshift, in contrast to the smaller redshift of the VBLR lines.

TABLE 3

COMPARISON OF EMISSION LINE REGIONS

	NLR	ILR	VBLR
Velocity Dispersion (km s^{-1})	~500	~2000	~7000
Radial Distance (pc)	10^{2-3}	~1	~0.1
Gas Density (n_H, cm^{-3})	10^{4-6}	$\sim 10^{10}$	$\sim 10^{12.5}$
Ionization Parameter (U)	~0.01	~0.01	~0.01
Redshift cf. Systemic (km s^{-1})	0	~0	~ −1000
Covering Factor ($\Omega/4\pi$)	$\lesssim$0.02	$\lesssim$0.03	~0.24

This systemic redshift is indicated in two independent ways. First, by the agreement in redshift of the peaks, between the broad lines of C IV λ1549, C III] λ1909, and Mg II λ2798 when these lines are narrowest (Brotherton et al. 1994), together with the very small average shift between Mg II λ2798 and the NLR lines thought to peak at the systemic redshift (Tytler & Fan 1992). Second, Heckman et al. (1991) have found that broad C IV emission is blueshifted by up to $\sim$1000 km s^{-1} relative to the emission from the extended Lyα nebulae in high-redshift radio-loud QSOs. This is just the amount that the C IV VBLR emission is blueshifted relative to the ILR emission. Thus ILR emission is at about the same redshift as the extended Lyα emission that, like the NLR emission, is almost certainly systemic.

2. Whittle (1992b) showed that, for NLR emission lines of Seyfert galaxies, the core widths ($\sim$600 km s^{-1}) strongly correlate with widths of the wings (FWHM $\sim$ 1200 km s^{-1}) (see also de Robertis & Osterbrock 1984). Also, Heckman et al. (1991) find velocity dispersions of 1000–1500 km s^{-1} in the Lyα nebulosities of QSOs. These widths approach ILR velocity dispersions. Whittle (1992a) presents strong arguments for a virial origin for these velocities, so we expect "NLR" gas closer to the nucleus to show ILR velocity dispersions approaching those observed or deduced (1500–2500 km s^{-1}).

3. The spectra and model calculations presented here strongly indicate ILR densities and nuclear distances intermediate between those of the NLR and VBLR, suggesting a link between them.

How distinct are the ILR and VBLR really? By far the simplest explanation for the statistical relations among line strength and profile parameters is that there is a region of low velocity dispersion that has different physical characteristics compared with the high-velocity VBLR, with a wider dispersion in the log EW of the ILR spectrum by a factor of 3 (Francis et al. 1994). The PCA is particularly powerful in demonstrating that the first principal component, representing all or most of the ILR emission, is essentially uncorrelated with VBLR emission. Although the regions may indeed merge, the characteristics of the ILR clearly differ from those of the VBLR.

In only a few objects, the NLQSOs, has it been possible to distinguish the individual ILR and VBLR profile components directly. In the three clear examples investigated by Baldwin et al. (1988), for the C IV line, the ILR FWHMs were about 1400 and 1550 km s^{-1}, and for the VBLR, 7200 and 8900 km s^{-1}. Their high ILR/VBLR intensity ratios are similar to those for the lines of smallest FWHM and largest EW investigated by Wills et al. (1993), and their spectra are like that of the ILR (Table 2). (See Kinney et al. 1987, and possibly Netzer, Wills, & Wills 1982, for two more examples.)

A similar kind of distinction is made between the NLR and BLR—the main differences being that in many cases the widths of the NLR and BLR emission lines in the optical are very different (e.g., 500 km s^{-1} compared with 5000 km s^{-1}) so that there is a clear inflection in the Hβ or Hα profile; in cases where the line widths are more similar, the more isolated [O III] lines betray the presence of a distinct NLR. In some nearby AGNs, it is possible to spatially resolve the NLR. For an ILR of the type we describe, none of these tests is available. A more sophisticated investigation, like our previous statistical work, is required to detect the presence of such a line.

If our notions about a link between the ILR and NLR are correct, then ILR and NLR line strengths should be correlated. As a test, we predict that, for example, the [O III] λ5007/Hβ line ratio will inversely correlate with the C IV line width (FWHM). Observations with the *Hubble Space Telescope* will allow this test in the very near future.

5. SUMMARY

We have analyzed the UV spectra (1100–2000 Å) of two high-luminosity ($M_B \sim -26.3$ and -28.2), high-redshift samples of predominantly radio-quiet QSOs and have shown that the line ratios of broad- and narrow-lined objects systematically differ. This immediately rules out simple orientation of models of the BLR that depend only on kinematic projection to explain different profiles. We have shown that the ILR and VBLR spectra are distinguished by very different line ratios.

Using photoionization models, we were able to find consistent solutions that reproduce the ILR line ratios, and that less successfully reproduce the VBLR line ratios. This is consistent with our previous conclusion (Brotherton et al. 1994) that the VBLR itself is probably less homogeneous than the ILR.

We have deduced the physical characteristics of the ILR and VBLR, which we summarize in Table 3. There, we also list the properties of the NLR for comparison. The velocity dispersions, densities, and covering factors appear to decrease with increasing distance from the central engine, while the ionization parameter remains approximately constant.

In previous papers we have used statistical relations between line strengths and profile parameters to deduce the existence of two regions—the ILR and VBLR. Here we have derived spectra allowing us to characterize these regions in terms of different, physically plausible parameters, further supporting the notion of a BLR composed of an ILR and a VBLR that are relatively distinct.

We thank W. L. W. Sargent for allowing us to use his data, Derek Wills for useful discussions, and Gary Ferland and Hagai Netzer for useful discussions and for providing us with

their photoionization codes CLOUDY and ION. B. J. W. and M. S. B. gratefully acknowledge support from grant HST GO-2578.01-87A RQ-Q, from the Space Telescope Science Institute, which is operated by AURA, Inc., under NASA contract NAS5-26555. The LBQS is supported by the National Science Foundation under grant AST 90-01181, for which we are grateful. P. J. F. acknowledges support from a NATO/SERC advanced fellowship and an ARC grant.

REFERENCES

Baldwin, J. A., Ferland, G. J., Carswell, R. F., Phillips, M. M., Wilkes, B., & Williams, R. E. 1994, in preparation
Baldwin, J. A., McMahon, R., Hazard, C., & Williams, R. E. 1988, ApJ, 327, 103
Brotherton, M. S., Wills, B. J., Steidel, C. C., & Sargent, W. L. W. 1994, ApJ, 423, 131
Chaffee, F. H., Foltz, C. B., Hewett, P. C., Francis, P. J., Weymann, R. J., Morris, S. L., Anderson, S. F., & MacAlpine, G. M. 1991, AJ, 102, 461
Clavel, J., et al. 1991, ApJ, 366, 64
de Robertis, M. M., & Osterbrock, D. E. 1984, ApJ, 286, 171
Ferland, G. J. 1986, in Workshop on Model Nebulae, ed. D. Pequignot (Paris: Observatoire de Paris), 319
———. 1987, in Rutherford-Appleton Workshop on Emission Lines in AGN, RAL-87–109, ed. P. M. Gondhalekar (Oxford: Rutherford Appleton Lab.), 107
———. 1993, Univ. Kentucky Department of Physics and Astronomy Internal Report
Ferland, G. J., & Osterbrock, D. E. 1986, ApJ, 300, 658
Foltz, C. B., Chaffee, F. H., Hewett, P. C., MacAlpine, G. M., Turnshek, D. A., Weymann, R. J., & Anderson, S. F. 1987, AJ, 94, 1423
Foltz, C. B., Chaffee, F. H., Hewett, P. C., Weymann, R. J., Anderson, S. F., & MacAlpine, G. M. 1989, AJ, 98, 1959
Francis, P. J. 1993, ApJ, 405, 119
Francis, P. J., Brotherton, M. S., & Wills, B. J. 1994, in preparation
Francis, P. J., Hewitt, P. C., Foltz, C. B., & Chaffee, F. H. 1992, ApJ, 398, 476
Hamman, F., & Ferland, G. J. 1992, ApJ, 391, L53
Heckman, T. M., Lehnert, M. D., Miley, G. K., & van Bruegel, W. 1991, ApJ, 381, 373
Hewett, P. C., Foltz, C. B., Chaffee, F. H., Francis, P. J., Weymann, R. J., Morris, S. L., Anderson, S. F., & MacAlpine, G. M. 1991, AJ, 101, 1121
Hooper, E. J., Impey, C. D., & Hewett, P. C. 1994, ApJ, in press
Kallman, T. R., Wilkes, B. J., Krolik, J. H., & Green, R. 1993, ApJ, 403, 45
Kinney, A. L., Huggins, P. J., Glassgold, A. E., Bregman, J. N. 1987, ApJ, 314, 145
Kriss, G. A., Davidsen, A. F., Blair, W. P., Ferguson, H. C., & Long, K. S. 1993, ApJ, 394, L37
Krolik, J. H., Horne, K., Kallman, T. R., Malkan, M. A., Edelson, R. A., & Kriss, G. A. 1991, ApJ, 371, 451
McCarthy, P. J. 1993, ARA&A, 31, 639
Mathews, W. G., & Ferland, G. J. 1987, ApJ, 323, 456
Mittaz, J. P. D., Penston, M. V., & Snijders, M. A. J. 1990, MNRAS, 242, 370
Morris, S. L., Weymann, R. J., Anderson, S. F., Hewett, P. C., Chaffee, F. H., Francis, P. J., & MacAlpine, G. M. 1991, AJ, 102, 1627
Netzer, H. 1985, MNRAS, 216, 63
Netzer, H., & Laor, A. 1993, ApJ, 404, L51
Netzer, H., Wills, B. J., & Wills, D. 1982, ApJ, 254, 489
Nussbaumer, H., & Story, P. J. 1982, A&A, 115, 205
Rees, M., Netzer, H., & Ferland, G. J. 1989, ApJ, 347, 640
Sargent, W. L. W., & Steidel, C. C. 1994, in preparation
Sargent, W. L. W., Boksenberg, A., & Steidel, C. C. 1988, ApJS, 68, 539
Sargent, W. L. W., Steidel, C. C., & Boksenberg, A. 1989, ApJS, 69, 703
Steidel, C. C., & Sargent, W. L. W. 1991, ApJ, 382, 433
———. 1992, ApJS, 80, 1
Tytler, D., & Fan, X. 1992, ApJS, 79, 1
Visnovsky, K. L., Impey, C. D., Foltz, C. B., Hewett, P. C., Weymann, R. J., & Morris, S. L. 1992, ApJ, 391, 560
Whittle, M. 1992a, ApJ, 387, 121
———. 1992b, in Testing the AGN Paradigm, ed. S. S. Holt, S. G. Neff, & C. M. Urry (AIP Conf. Proc. 254), 607
Wills, B. J., Brotherton, M. S., Fang, D., Steidel, C. C., & Sargent, W. L. W. 1993, ApJ, 415, 563

Note added in proof.—The third sentence of the last paragraph in § 4.2 should read: "In QSOs dominated by the VBLR, the ILR spectra are weaker leading to correspondingly smaller ILR covering factors."

Our ILR and VBLR designations are related to the BLR I BLR II designations of Gaskell (1987, in Astrophysical Jets and Their Engines, ed. W. Kundt, Dordrecht: Reidel, 29), although the level of detail and interpretation of these designations differ.

Also, we noticed an error in Brotherton et al. (1994). The last line in the fourth paragraph of § 1 should conclude, "... Lyα and C IV have larger EWs and smaller FWHMs in radio-loud QSOs than in radio-quiet QSOs."